Supporting Information for

Exclusively Proton Conductive Membranes Based on Reduced Graphene Oxide Polymer Composites.

Dhanraj B. Shinde,[1] Ivan V. Vlassiouk,[2] Marat R. Talipov[1] and Sergei N. Smirnov[1]*

[1] Department of Chemistry and Biochemistry, New Mexico State University, Las Cruces, NM 88003, United States

[2]Oak Ridge National Laboratory, Oak Ridge, Tennessee 37831, United States

E-mail: snsm@nmsu.edu

I.   *Preparation Details*

To prepare a composite membrane, the desired polymer powder was added to an aqueous 0.4 wt% dispersion of graphene oxide (from Graphenea). For example, when 40 mg of polyvinyl pyrrolidone (PVP) were added to 10 mL of 0.4% GO solution, the resulting PVP/GO (in the 1:1 ratio) solution was produced. The solution was sonicated for 10 minutes in a bath ultra sonicator (VWR 40 kHz, 48 W) to form a homogeneous dispersion. Subsequently, 0.75 mL of that (PVP/GO) solution was vacuum filtered on a 1.5" PET hydrophobic support membrane (with 100 nm pores). A slightly wet PVP/GO film on the PET support was reduced in HI (54%) vapor at 95 °C for 24 h. Afterwards, the obtained r(PVP/GO) membrane was peeled from the PET membrane. The membrane was repeatedly rinsed with ethanol and water to remove residual HI.

Concentration of PVP and GO in the filtrate was measured by optical absorption. Absorbance at 213 nm was used for PVP and 500 nm for GO. We observed less than 2% of PVP in filtrate when 3.5 kDa PVP was used, even smaller amounts were observed for the same compositions using higher MW PVP. Thus, most of PVP remains in the film and resulting PVP/GO membrane has practically the composition as in solution. Other methods for films preparation were also investigated but they showed inferior to vacuum filtration performance, at least when proton selectivity was used as the main metric for characterization.

As shown in Fig. 2a, the resulting r(PVP/GO) membrane is well packed and measures 11 μm in thickness, which corresponds to *ca.* 1.4-2.0 nm distance between the rGO sheets. The latter was estimated from 4 mg/mL of GO in solution, 0.75 mL of which was spread over 3.8 cm diameter filter.

Other means of preparing the film, Dr. Blade casting and evaporation from a Teflon beaker, did not yield membranes with as high selectivity. Nevertheless, Dr. Blade casting on a PET film yielded much better results compared to casting on glass. (Table S1). Such sensitivity to seemingly minor experimental parameters reflects the importance of the multiple features. First, accessing both sides of the membrane during reduction when on PET membranes allows more uniform (and faster) reduction. Second, alignment of GO flakes by unidirectional water flow in vacuum filtration also establishes pathways that are later employed in the reduction process.

Table S1. OCV* data for pH1/pH2 gradient for different methods of preparation of the same composite membrane formulations, 0.65 PVP/GO and reduction for 24 h in HI vapor.

Membrane composition and preparation method	Zero salt (mV)	1M KCl (mV)
Vacuum filtration	59	52
Dr. Blade on a glass	39	5
Dr. Blade on a PET membrane	56	39
Spin coating	59	35
Slow evaporation in Teflon beaker	39	5

* - all values are given with the accuracy *ca.* 1 mV

The size of GO platelets also affects the performance and excessive sonication with ultrasound tip, which causes a decline in the platelets' size, reduced the performance. For example, after treatment with ultrasound horn to the total energy density 14.4 kWh/L the OCV at ΔpH=1 and 1 M KCl in a typical r(PVP/GO) membrane drops down to 32 mV. For that reason, we used only sonication bath and Graphenea a reproducible source of GO.

Table S2. OCV* data for pH1/pH2 gradient for different composite membrane formulations

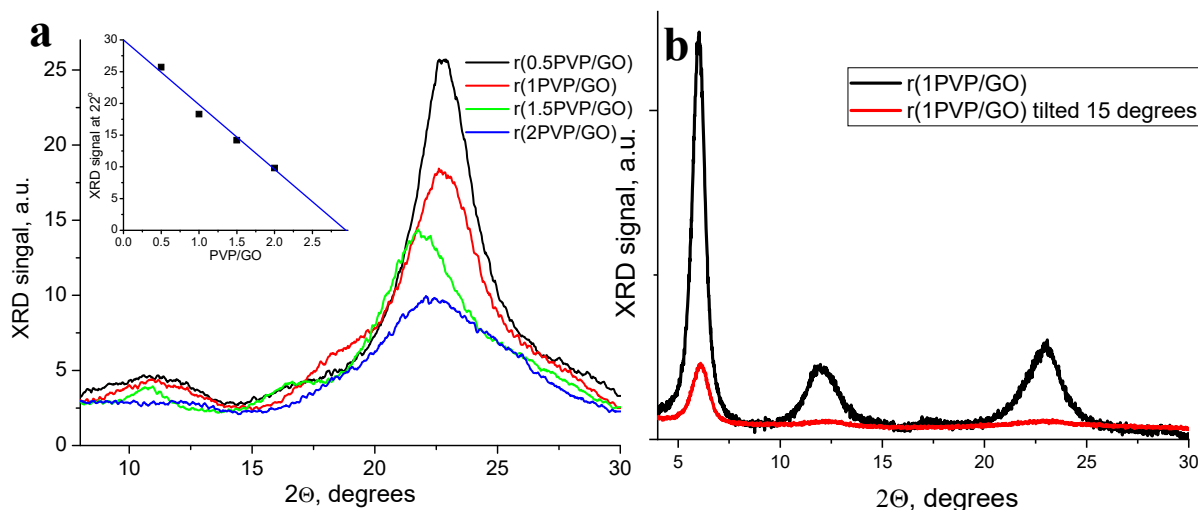| Membrane composition and preparation method	Zero salt (mV)	1M KCl (mV)
Membranes reduced by HI vapor		
GO + HI 24 h, rGO	39	6
PVP/GO=1 + HI 2 h	56	46
PVP/GO=1 + HI 24 h, r(PVP/GO)	59	52
PVP/GO=1 + HI 48 h	59	52
MVP/GO=1 + HI 24 h	56	32
CL/GO=1 + HI 24 h	58	38
NMCL/GO=1 + HI 24 h	58	39
PVA/GO=1+HI 24 h	56	24
PAA/GO**=1 + HI 24 h	35	5
SDBS/GO=1 + HI 24 h	33	5
PEG/GO=1+ HI 24 h	34	5
PVPY/GO=1+HI 24 h	34	5
SDS/GO=1+HI 24 h	39	6
Other types of membranes		
PVP/GO=1 + HBr 24 h	56	15
A small open pore	35	4
GO	33	5
Nafion 212	59	5
Nafion 117	59	4

PVP = polyvinylpyrrolidone, MVP = (mono) vinylpyrrolidone, CL = ε-caprolactam, NMCL = N-methyl caprolactam, PVA = poly vinyl alcohol, PAA= polyacryl amide, SDBS = sodium dodecyl benzene sulfonate, SDS = sodium dodecyl sulfate, PVPY= Poly-4-vinyl pyridine, GO = unreduced graphene oxide

* - all values are given with the accuracy $\pm$1 mV

**- the membrane is not uniform and fragile

II.   *XRD Analysis*

X-ray diffraction patterns for membranes were obtained using a PANalytical Empyrean X-Ray Diffractometer with Cu Kα line generated at 40 kV and 40 mA. The samples were placed on a glass slide and recorded using 4° min^{-1} scan rate with the step size of 0.02°.
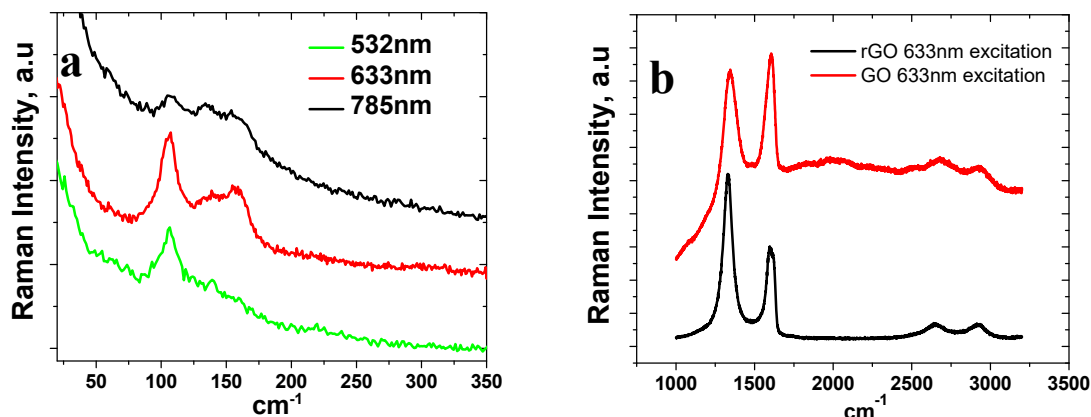

Figure S1. **a.** XRD for composite films prepared from (PVP/GO) in different proportions after reduction with HI. The insert illustrates the variation of the intensity at 22° on the PVP/GO ratio. **b.** XRD of r(1PVP/GO) and same sample tilted by 15°.

Low angle diffraction peak (~6°) in PVP/GO and r(PVP/GO) composites is assigned to the (001) d-spacing between either GO or rGO sheets with PVP in between, and the peak at twice the angle of the first one (~12°) is the (002) reflection. Overlapping not reduced GO patches without PVP in between also may contribute to this peak (**Fig. S1**). The peak at 22° is assigned to overlapping rGO-rGO sheets without polymer in between, (refs. 9-15) which is supported by the decrease of this peak intensity with increasing PVP fraction (**Fig. S1**). A decline of the peaks' intensity for tilted sample together with well defined (001) and (002) peaks suggest that GO and rGO sheets are well packed in a nacre-like structure, as well as, points that majority of GO sheets are individually dispersed in the PVP matrix and retain such dispersion after reduction, without forming multilayer rGO stacks. Reduction of PVP/GO composites does not result in significant decrease of the interlayer distance (<1 Å) in contrast to reduction of pure GO membrane (~5 Å) (**Fig. 1a,b**), suggesting a noticeable uptake of I$_3^-$ along with possible reorganization of PVP.

III.   Raman Analysis

The representative membranes were analyzed using a Renishaw inVia Qontor micro-Raman spectrometer equipped with 532, 633, and 785 nm lasers operating at 1-10% power. Multiple points across membrane area were checked confirming samples' uniformity.
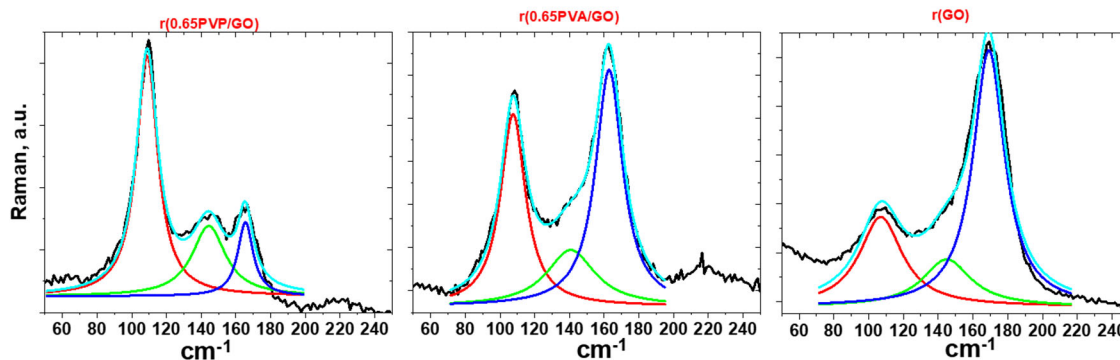

Figure S2. **a.** Raman spectra of r(0.65 PVP/GO) in the low frequency region with different excitation energies. Note strong dependence of the relative intensities of 110 and 170 cm^{-1} lines from different forms of iodine. **b.** Raman spectra in the 1000-3200 cm^{-1} range for GO membrane before and after reduction.

Triiodide can be detected by its characteristic Raman signal at 110 cm^{-1}, as opposed to the I_2 signal at 170 cm^{-1} and by XPS (see **Figs. 1c, S2**). **Figure S2** shows Raman spectra of different samples reduced with HI, where different intensities of these peaks can be clearly seen for them. It is known that solid I_2 [d (I-I) = 2.715 A] shows a peak near 180 cm^{-1} which moves towards lower frequencies when I_2 interacts with donors to form charge-transfer (CT) complexes. The Raman at 110 cm^{-1} is assigned to the active symmetrical stretching in I_3^- a peak. The peak in between, at 145 cm^{-1}, is believed to correspond to either the outer I-I stretching in a bent I_5^- or to asymmetric I_3^-, or the Fermi resonance between v_1 and $2v_2$ in symmetrical I_3^-, *i.e.*, both I_3^- and/or I_5^- species can contribute to it.[S1-S2] We see a correlation between the 110 and 170 cm^{-1} peak ratio (I_3^-/I_2) and the proton selectivity of composite. Indeed, the ratio is the highest (3.2) for r(PVP/GO) and decreases to 0.8 and 0.35 or r(PVA/GO) and rGO, respectively; see deconvolutions in **Fig. S3**. Similar trend is observed for the 145 and 170 cm^{-1} intensities ratio ($I_{3/5}^-/I_2$) which declines in the order 1.05, 0.23, and 0.18 for r(PVP/GO), r(PVA/GO) and rGO, respectively. Increasing the excitation wavelength results in a lower I_3^-/I_2 peak ratio, which correlates with I_2 having absorption maximum at the longer wavelength (~500nm), as compared to I_3^- and I_5^- species.[S3]

The main features in the Raman spectra of GO and rGO are the so-called *G* and *D* peaks, which come at around 1560 and 1360 cm^{-1}, respectively. The ratio of I_D/I_G gives the information about the average distance between the defects. For example, the r(PVP/GO) sample shows I_D/I_G ~ 1.8 for 633 nm excitation corresponding to the average distance ~2 nm between the defects and the density of these defects decreases upon reduction but their density remains high. The type of
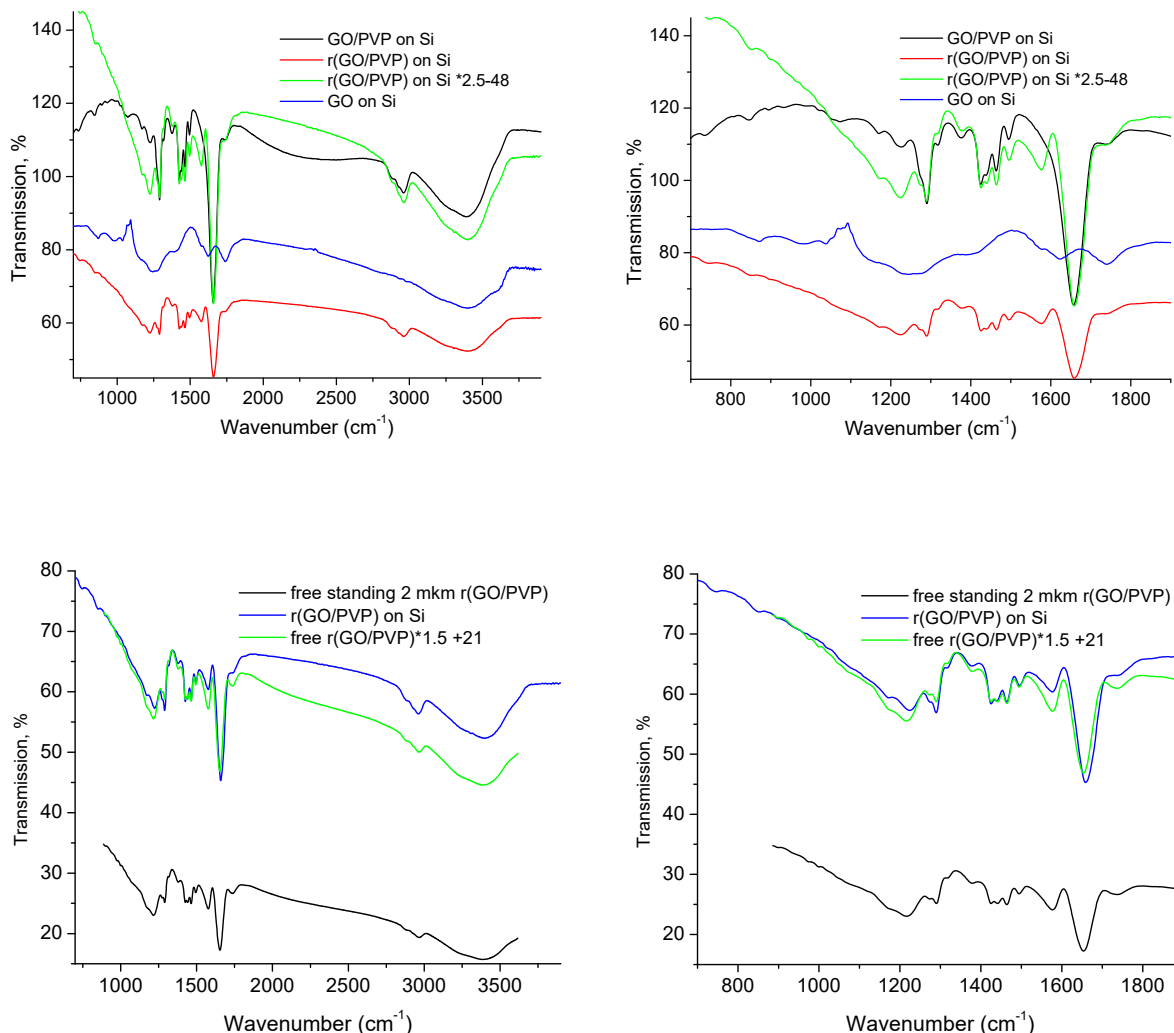
such defects cannot be recovered from the Raman spectra directly and thus their role in proton conductance is not obvious but would be highly desirable for understanding the overall phenomenon. We believe, the contribution to the overall proton conductance from such defects is significant as the proton selectivity declines upon decreasing the size of GO sheets with rigorous ultrasound treatment.

Figure S3. Deconvolution of Raman spectra of different composite films from Fig. S2a: rGO, r(0.65PVA/GO), r(0.65PVP/GO), in the low frequency region with 532 nm excitation. Fitting of the low energy part of Raman spectra shows three bands: ~110cm^{-1} (I_3^-, red), ~145cm^{-1}, (I_3^-/I_5^-, green) and ~170cm^{-1} (I_2, blue).

IV.   FTIR Analysis

FTIR spectra were recorded using Nicolet iS10 spectrometer in a transmission mode. Two types of samples were investigated showing matching results: free standing membrane films and films on Si wafer. Free standing r(PVP/GO) membranes were thinner (~2 μm) but otherwise identically produced to standard membranes. Films on Si wafers were casted using spin coating of the same solutions using low rpm to achieve noticeable thickness. The background signals were, correspondingly, empty opening and an Si wafer exposed to the same treatment but without the film.
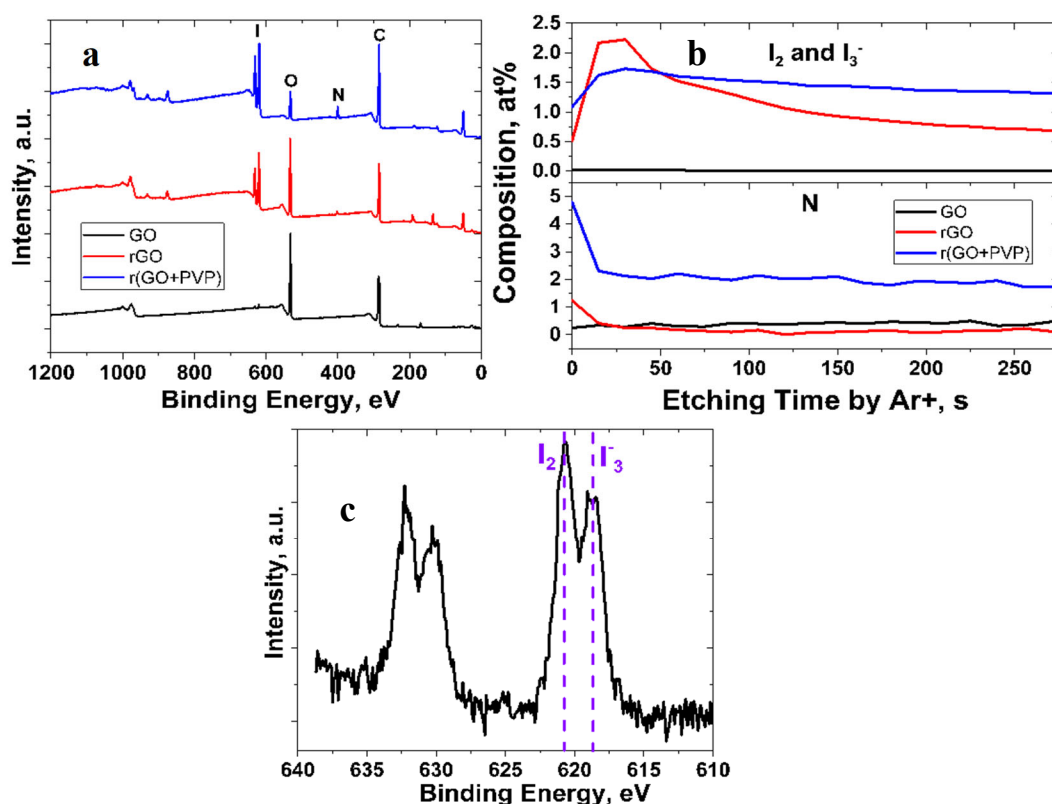

Figure S4: FTIR spectra of different films on two different scales. The agreement between the free standing r(PVP/GO) film and that on Si wafer indicate that the changes in the latter with reduction are not due to the substrate. The signal for rGO film is not shown on this scale as it corresponds to zero transmittance.

Three things come out from analyzing the spectra in **Fig. S4**. First, when rGO flakes contact each other continuously, they have metallic appearance and reflect very well IR radiation in the whole range. When rGO flakes are separated (partially or in full) by PVP, the reflection of IR is less effective, especially at low frequencies. Second, spectral features for the free-standing r(PVP/GO) and for such membrane prepared on Si are identical. Third, the intensity of the most pronounced carbonyl peak of PVP decreases after reduction by a factor of *ca.* 2.5. According to Goodwin *et al.*,[22] complexation of PVP with HI_3 in stoichiometry 2PVP monomers per one HI_3 causes disappearance of the carbonyl signal and appearance of a wide peak at around 760 cm^{-1}. We do not see the latter because of the above-mentioned increase of transmittance in r(PVP/GO) at low frequencies. The carbonyl signal decline can be used to estimate the PVP:HI_3 stoichiometry as roughly one HI_3 per 4-5 monomer PVP units.
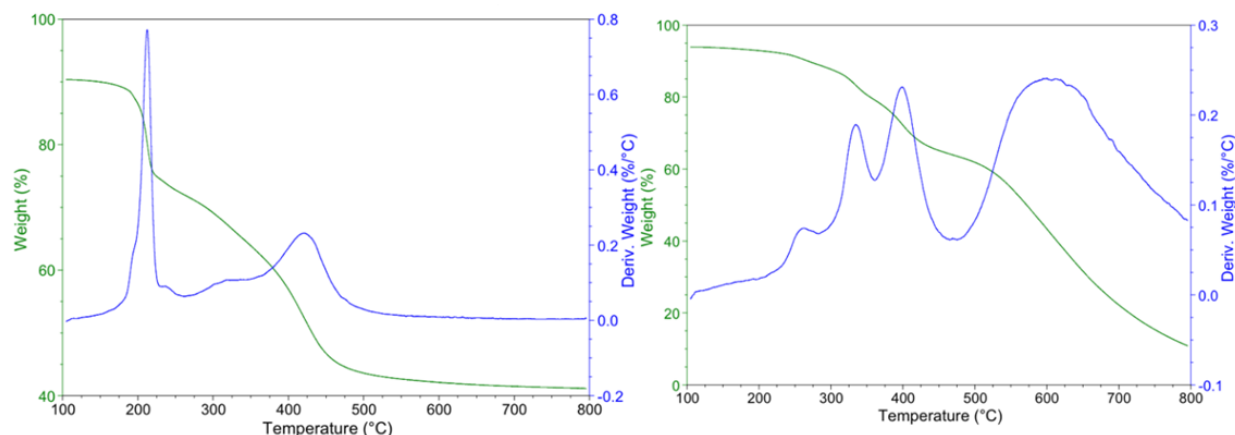
V. XPS Analysis

X-ray photoelectron spectra (XPS) were acquired using Thermo Scientific Model K-Alpha XPS instrument. The spectra were obtained using micro-focused, monochromatic Al Kα X-rays (1486.6 eV) with 400μm X-ray spot size. Depth profiles were measured using a monoatomic Ar-ion source operated at 2kV ion energy. The sputter rate was calibrated using standard thickness SiO_2 films and was ~12 nm/min. Data were collected and processed using the Thermo Scientific Advantage XPS software package.

Figure S5. **a.** Survey XPS spectra showing chemical composition of dropcasted films. Major elements are marked on the top: I, O, N, and C. **b.** Depth profile analysis demonstrating presence of nitrogen in the films only for r(PVP/GO) sample, while iodine species were detected for both r(GO) and r(PVP/GO). Data is shown for dropcasted films of GO (black), rGO (red) and r(PVP/GO) (blue). **c.** XPS spectrum of iodine species region showing evident bands for I_2 (~620.5eV) as well as I_3^-(618.7) supporting conclusions of Raman analysis in Figs. 1c, S2, and S3. Spectrum was obtained on r(0.65PVP/GO) membrane that showed OCV~50mV. As expected, the surface composition of prepared films contains I, O, N, and C, as proved by XPS spectra (Figure S5a). Casted films' depth profile analysis suggests that nitrogen exists only in r(PVP/GO) film (from PVP polymer), while iodine is present in both reduced r(GO) and r(PVP/GO) films (Figure S5b). Both I_2 (~620.5eV) and I_3^-(618.7) were detected confirming Raman assessment in **Figs. 1c**, **S2**, and **S3**. Assignment of the iodine species bands was done according to the previous reports.[20,21] Based on the composition profile, the ratio of atomic % for N and I is approximately N:I = 2:1.5, which corresponds to roughly one I_3^- per four PVP monomer units.
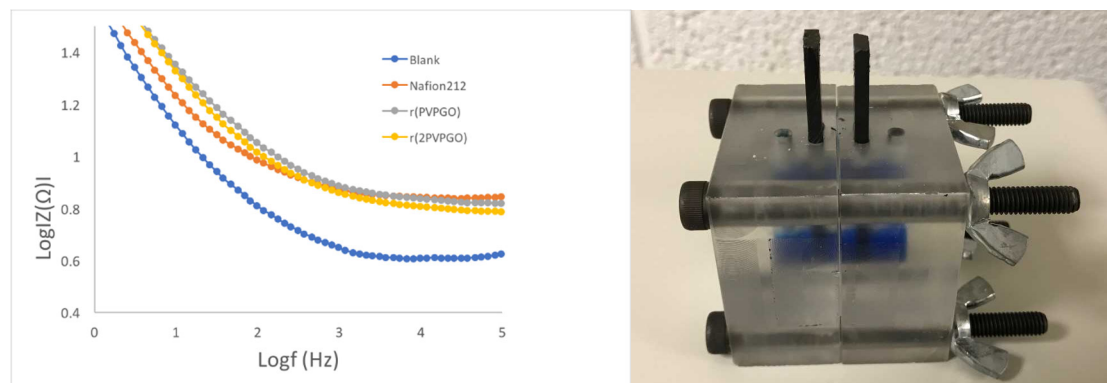
VI. TGA Analysis

Figure S6: Thermogravimetric analysis (TGA) and the derivative curves for PVP/GO and r(PVP/GO) samples, saturated with water and measured in Ar atmosphere in the temperature range 100 to 800 °C.

Thermogravimetric analysis (TGA) measurements were carried out on a Thermal Analysis (TA) Instruments Q500 analyzer. The samples were placed in platinum pans and the temperature ramps were performed using heating rate of 10 °C/min under 20 sccm flow of nitrogen. Temperature ramps were performed after equilibrating the samples at 105 °C for 20 min in order to remove bulk water. The TGA and the derivative (DTG) curves in **Fig. S6** for PVP/GO and r(PVP/GO) membranes are quite different, the latter demonstrates a better thermal stability with no significant variation till 300 °C. The samples were kept at 105°C for 20 min to reduce the amount of water, which is reflected in a lower mass at the starting point of 100°C. This loss of water is greater in PVP/GO (10%) than in r(PVP/GO) (6%). Moreover, there is noticeable difference in the step at 200 °C representing the decomposition of –COOH and OH groups in graphene oxide of PVP/GO sample, whereas no such major weight loss is observed for r(PVP/GO) confirming a complete reduction of GO with HI vapor treatment. Also, PVP decomposes in the temperature range up to 450°C,[S4] which is observed in both samples and implies almost the same amount of PVP in them. The additional loss close to 50% at higher temperatures for r(PVP/GO) sample is due to presence of iodine. Such a high temperature for iodine loss indicates its strong interaction with PVP and rGO. The amount of iodine can vary depending on conditions; the estimate based on one HI_3 per two PVP units suggests *ca.* 1.7 times greater the amount of iodine compared to PVP, which is close to the experimental.
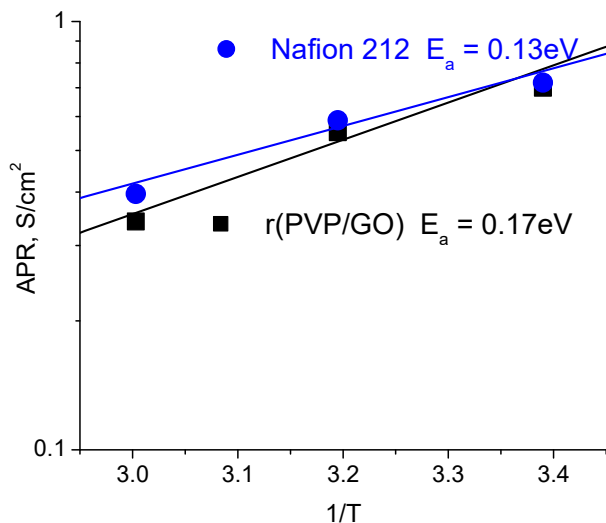
VII. Proton Conductance

To eliminate contribution from the electrode reactions, the proton conductance was measured in the AC impedance mode performed with a CH 604B electrochemical workstation (from CH Instruments). A homemade PMMA cell (see **Fig. S7**) had two compartments (0.5 mL) separated by a membrane of interest with 1 cm^2 cross section using and a graphite electrode on each side close (3 mm) to it. The impedance was measured at a low voltage (5 mV AC) and for frequencies from 0.1 Hz to 10^5 Hz. A typical VRB electrolyte, *i.e.*, 1.5M $VOSO_4$+3M H_2SO_4, or just 3M H_2SO_4 were used. Frequency dependence of the impedance in all cases shows a capacitive region due to electrodes at low frequencies which declines with increasing frequency and eventually saturates at the resistive part where the reading for resistances were taken. First, the electrolyte solution resistance, R_{sol}, was measured and its value is then subtracted from the resistance measured with membrane to obtain the membrane resistance. All measurements for different PVP/GO ratio were normalized by the total mass used for the membrane preparation and the area (0.3 cm^2) of membrane opening area. The proton conductance for Nafion212 was measured under identical conditions. Comparison to Nafion 212 was chosen because of the reported advantage of Nafion 212 over other Nafions in VFB applications.[S5,S6]

Figure S7: Proton conductance measurements setup based on a homemade PMMA cell with two compartments separated by a membrane and graphite electrodes on each side; the blue color is from the VRB electrolyte, 1.5M $VOSO_4$+3M H_2SO_4. Representative impedance frequency dependence traces show the resistive part at high frequency and the capacitive contribution at low frequency due to polarization at the electrodes. Increase in the resistive part due to membranes is clearly seen.

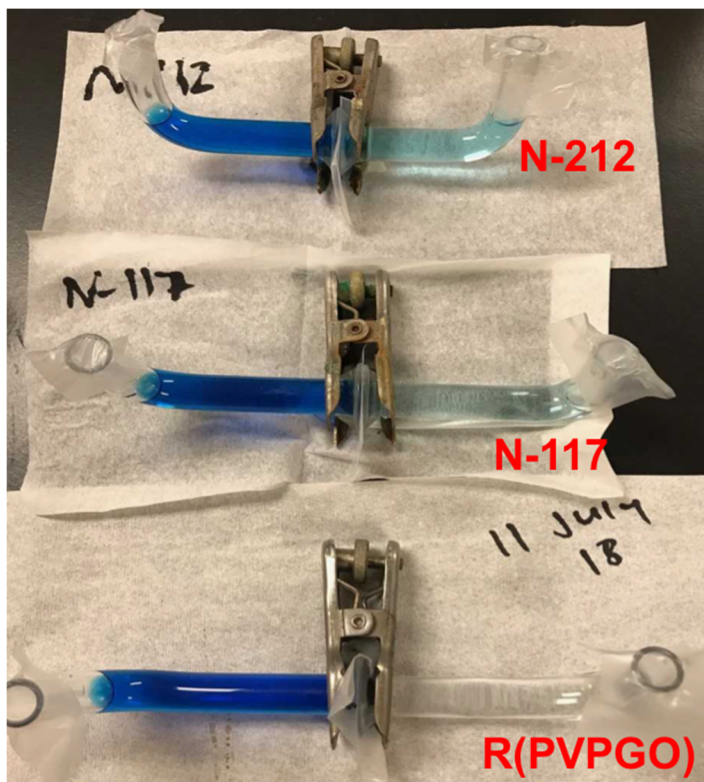## VIII. *Temperature Dependence of the Area Proton Resistance*

For temperature dependence, the same cell with electrolyte was placed in an oven with controlled temperature. The activation barrier for r(PVP/GO) is a bit greater than for Nafion, 0.17 eV *vs* 0.13 eV, making r(PVP/GO) further advantageous at elevated temperatures.

Figure S8: Temperature dependence of APR (area proton resistance) in 1.5M $VOSO_4$ + 3M H_2SO_4 electrolyte measured at 100kHz for Nafion 212 and r(PVP/GO).
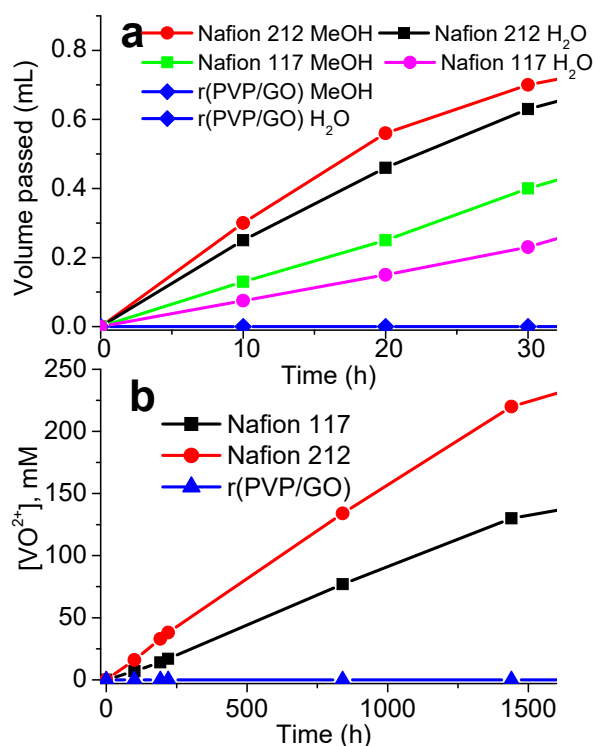
IX. Crossover Experiments

The VO^{2+} permeability of a membrane was measured using a glass U-tube cell/diffusion cell, which was filled with 1.5M $VOSO_4$ solution (V_A = 4 mL) in one compartment and 1.5M $MgSO_4$ solution in the other compartment (V_B = 4 mL), respectively. As **Fig. S9** illustrates, only r(PVP/GO) membrane has no crossover of vanadium.

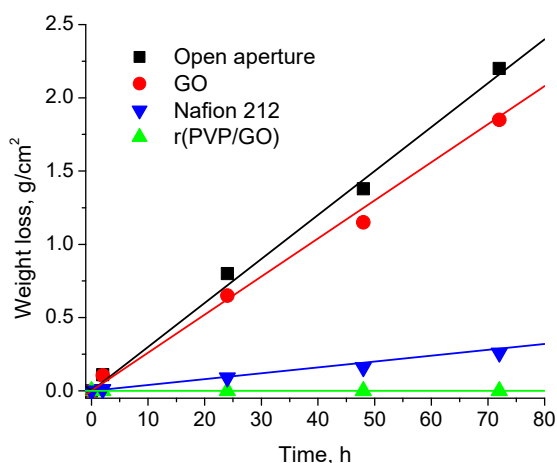**Figure S9**: Illustration of the vanadium crossover experiments with U-tubes filled with 1.5M $VOSO_4$ in one compartment and 1.5M $MgSO_4$ in the other. It is clearly visible that blue-colored VO^{2+} ion most effectively passes through Nafion 212 membrane while no coloration is detected for our r(PVP/GO) membrane. As a matter of fact, that very setup still does not show any coloration after 10 months.

Since neither ions, cations or anions, move through our membrane, water crossover experiments can be carried out also using a similar U-tube cell with 1M NaCl solution in one compartment and the same volume (4 mL) of water in the other.

Water practically does not move through our membranes, but it does through Nafion. Because in methanol/water mixture crossover of water in Nafion is significantly suppressed,[S7] methanol crossover experiments can be carried out in a similar manner for both using a similar U-tube cell with 1:1 water : methanol solution (12.5M) in one compartment and the same volume of water in the other.
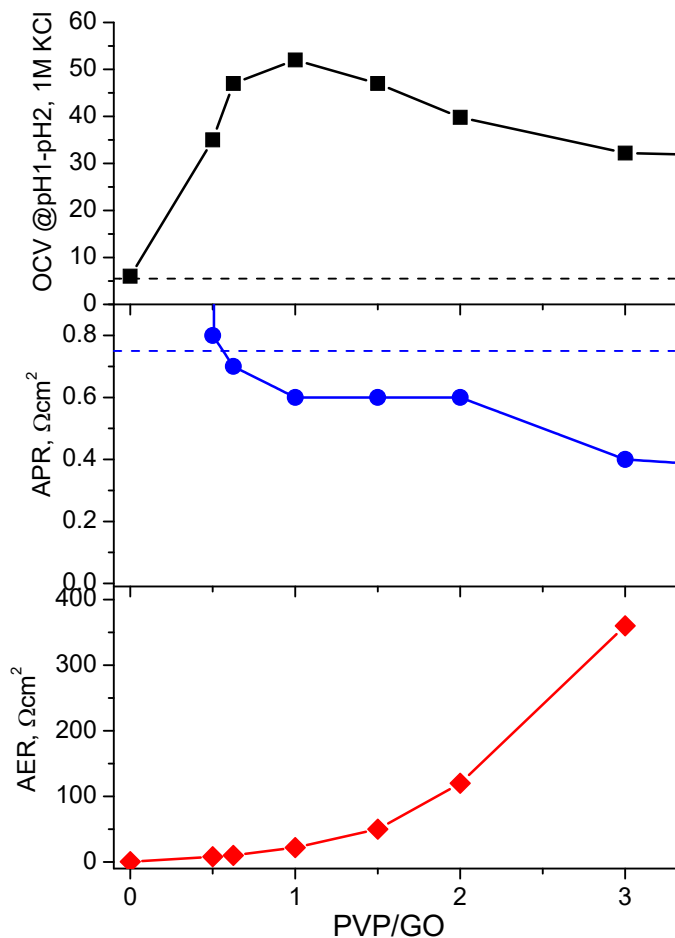
Figure S10: a. Crossover of MeOH from 50/50 aqueous solution into water through 0.3 cm^2 of Nafion 212 and r(PVP/GO) membranes. There is no detectable crossover of MeOH through r(PVP/GO) after 3 days. **b.** Crossover of VO^{2+} through 0.3 cm^2 of Nafion 212, Nafion 117, and r(PVP/GO) membranes between isotonic solutions of 1.5M VOSO$_4$ + 3M H$_2$SO$_4$ and 1.5M MgSO$_4$ + 3M H$_2$SO$_4$. There is no detectable crossover of vanadium through r(PVP/GO) even after 10 months. Low MW PVP (3.5 kDa) was used in all cases.

Figure S11: Crossover of water vapor across different membranes.
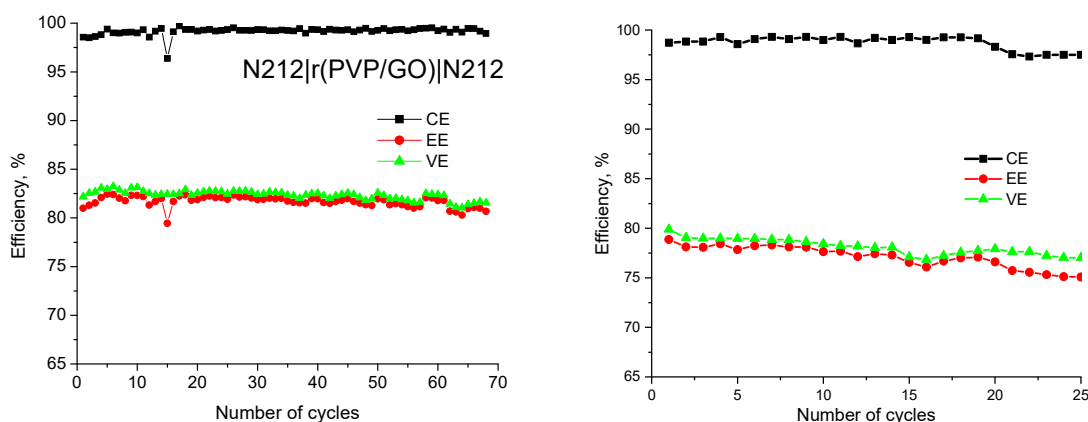
13

X. *Effect of PVP Fraction on Performance*

Increase of PVP fraction in r(xPVP/GO) composite membrane decreases the area proton resistance (APR) and almost exponentially increases the area electron resistance (AER), while the OCV has a pronounced maximum for PVP/GO~1. The electronic conductance primarily goes through overlapping rGO sheets without polymer in between, The corresponding XRD signal at 22° in Fig. S1a declines with increasing amount of PVP.

Figure S12. The OCV at 1M KCl for pH1/pH2 gradient (**a**), area proton resistance (APR) in 1.5M $VOSO_4$ + 3M H_2SO_4 electrolyte measured at 100kHz (**b**), and area electronic resistance (AER, **c**) for membranes with different PVP/GO ratios (normalized to the same mass). Low MW PVP (3.5 kDa) was used in all cases. The dashed lines show values for for Nafion 212 at the same conditions.

XI. Vanadium Flow Battery Experiments

Flow battery studies under load were performed using a cell from "Scribner Associates" with 5 cm^2 membrane area and serpentine flow channels. The carbon felt electrodes (4.6 mm thick, from SGL) were thermally activated at 450 °C for 20 hours in air. The negative and positive electrolytes, 30 mL of 1.5 M V(III) and V(IV) sulfate in 3M H$_2$SO$_4$, respectively, were kept under the nitrogen atmosphere. The electrolyte solutions were driven through the VRFB cell by a double peristaltic pump (from MTI) with a flow rate of 60 mL min^{-1}. The charge and discharge of the cell was controlled using a VSP galvanostat/potentiostat (from Bio-Logic) via Galvanostatic Intermittent Titration Technique with the cut-off voltages adjusted for the iR drop for a particular membrane: 1.65 V and 0.8 V for a double N-212 membrane and 1.75 - 0.6V for N-212| r(PVP/GO)| N212 membrane, respectively. The latter corresponds to r(PVP/GO) membrane sandwiched between the two N-212 sheets. A double N-212 sheet was chosen to better mimic the sandwich with r(PVP/GO), The two membranes had the resistance of 0.46 Ω and 0.32 Ω at the beginning of the test, as measured inside the battery using impedance spectroscopy. The capacity in each case was calculated by the software. The Coulombic efficiency (CE), voltage efficiency (VE) and energy efficiency (EE) of VFB were calculated by Eq. (3-5)
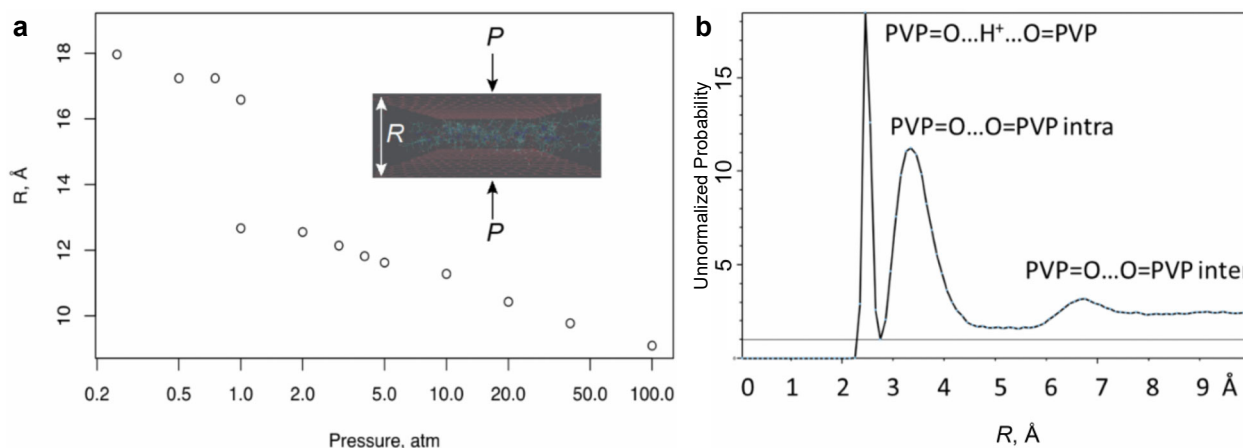

Figure S13. The coulombic (CE), voltage (VE), and energy (EE) efficiency for the 30mL VFB cell with 1.5M VOSO$_4$ + 3M H$_2$SO$_4$ as a function of number of cycles in two configurations from Fig 5a: two N212 membranes and r(PVP/GO) membrane sandwiched between the two N212 membranes.

XII. Molecular Dynamics Simulations

The initial structure of the membrane fragment was prepared by placing two fully overlapping 42×42 Å^2 graphene sheets with initial separation of 30 Å and randomly filling the space between them with 100 water molecules, 12 monoprotonated PVP6 molecules, and 12 triiodide ions using Packmol[S8] software. The obtained initial structure was pre-processed by Moltemplate[S9] software to generate input files for LAMMPS[S10] software. The molecular dynamics simulations were performed using LAMMPS software using 3D periodic boundary conditions with the periodic boundary box size of $46 \times 46 \times 46$ Å. The TIP3P model[S11] with fixed O-H bond lengths[S12] was used for the water molecules, and GAFF[S13] force field was used for other molecules in the assembly. The simulation was performed for 100 ns (time step 1 fs) using the NVE ensemble and Langevin dynamics. Atmospheric pressure was applied to the top and bottom graphene layers at $T = 298$ K (see **Figure S14**). The VMD[S14] software was used for the visualization and analysis of the resulting trajectories.

Figure S14: **a.** Distance between the graphene sheets as a function of pressure for the composition water: hydrogen triiodide: PVP: graphene = 2 : 4: 11 : 10 by mass. The effect of applied pressure on the d-spacing between graphene layers. The d-spacing of approximately 17 Å, observed at low pressures, corresponds to the presence of two layers of PVP in between two graphene layers. Higher pressure leads to the formation of a single PVP layer assembly with the characteristic distance of ~12 Å. Note that the replacement of graphene layers by rGO is expected to increase the d-spacing by ~2-3 Å due to the presence of oxygen atoms and various defects in rGO. **b**. Distribution of distances between oxygen atoms of PVP (intra- and inter-molecular) in the same assembly at 0.5 atm.

XIII. DFT Calculations of the pK$_a$ Shifts

Density functional theory (DFT) calculations were performed with the Gaussian 09 package, revision E01,[S15] at the PBE0/def2-SVP[S16] level of theory. Solvent effects were included using the SMD variation[17] of implicit integral equation formalism polarizable continuum model (IEF-PCM).[S18-S19] In all DFT calculations, ultrafine Lebedev's grid was used with 99 radial shells per atom and 590 angular points in each shell. Tight cutoffs on forces and atomic displacement were used to determine convergence in geometry optimization procedure. Hessians were calculated for the optimized structures of all neutral and cation radicals to confirm absence of imaginary frequencies.
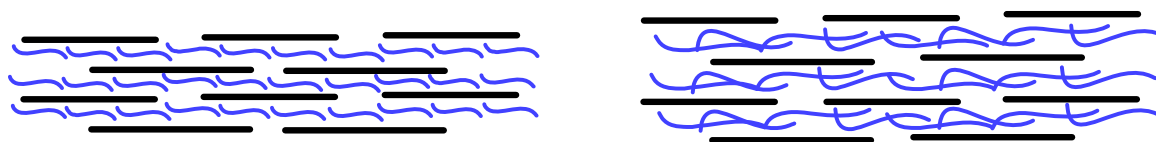
Table S3. Computed pKa shifts (relative to the pKa of H$^+$[N-Ethyl-2-pyrrolidone]) of various acids [PBE0/def2-SVP, SMD solvation model]

Acid	Benzene $\varepsilon = 2.3$	DCM[b] $\varepsilon = 8.9$	Acetone $\varepsilon = 20.5$	MeCN $\varepsilon = 35.6$	Water $\varepsilon = 78.4$	Exp (water)
H$^+$[acetone] [a]	-10.8	-7.6	-8.0	-7.7	-5.1	
H$^+$[methylacetate] [a]	-13.6	-10.2	-11.5	-10.1	-7.4	
H$^+$[2-pyrrolidone] [a]	-1.5	-0.6	-0.6	-0.5	-0.1	
H$^+$[acetamide-N-dimethyl] [a]	-0.4	1.5	1.2	1.2	1.5	
H$^+$[acetamide-N-methyl] [a]	-0.7	0.9	0.8	0.7	0.5	
H$^+$[acetamide-NH$_2$] [a]	-1.7	-0.7	0.2	0.5	0.2	
H$^+$[N-methyl-caprolactam] [a]	0.9	1.0	1.1	1.2	1.6	
H$^+$[caprolactam] [a]	0.4	0.7	0.8	0.8	1.1	
H$^+$[(H$_2$O)$_1$]	-24.6	-15.4	-16.6	-14.7	-5.9	-1.7
HI$_3$	12.8	-5.9	-12.0	-12.4	-13.1	
HBr$_3$	20.9	-1.8	-5.5	-7.1	-7.8	
HI	28.8	0.7	-4.1	-6.1	-7.1	-10
HBr	45.0	19.4	15.0	13.1	12.5	-9

[a] - Proton was placed on the carbonyl oxygen atom

[b] – Dichloromethane

Figure S15. Illustration of the effect of PVP (blue) length on selectivity in composite with rGO (black): shorter polymer on the left is neatly packed into a monolayer while the long one on the right has the polymer chains crossing each other and hindering neat packing.

References:

S1.   Svensson, P.H.; Kloo, L. Synthesis, Structure, and Bonding in Polyiodide and Metal Iodide−Iodine Systems. *Chem. Reviews* **2003**, *103*, 1649-1684.

S2.   Nour, E.M.; Chen, L.H.; Laane, J. Far-Infrared and Raman Spectroscopic Studies of Polyiodides. *J. Phys. Chem.* **1986**, *90*, 2841-2846.

S3.   Buckles, R.E.; Yuk, J.P; Popov, A.I. The Stability of the Tetramethylammonium Polyiodides in Ethylene Chloride. *J. Am. Chem. Soc.* **1952**, *74*, 4379-4381.

S4.   Zhu, K.; Wang, G.; Zhang, S.; Du, Y.; Lu, Y.; Na, R.; Mu, Y.; Zhang, Y. Preparation of Organic–Inorganic Hybrid Membranes with Superior Antifouling Property by Incorporating Polymer-Modified Multiwall Carbon Nanotubes. *RSC Adv.* **2017**, *7*, 30564-30572.

S5.   Reed, D.; Thomsen, E.; Wang, W.; Nie, Z.; Li, B.; Wei, X.; Koeppel, B. Sprenkle, V. Performance of Nafion® N115, Nafion® NR-212, and Nafion® NR-211 in a 1 kW Class All Vanadium Mixed Acid Redox Flow Battery. *J. Power Sources* **2015**, *285*, 425-430

S6.   Zhou, Y.; Yu, L.; Wang, J.; Liu, L.; Liang, F.; Xi, J. Rational Use and Reuse of Nafion 212 Membrane in Vanadium Flow Batteries, *RSC. Adv.* **2017**, *7*, 19425-19433

S7.   Barragán V.M.; Ruiz B.C.; Villaluenga J.P.G.; Seoane B. Transport of Methanol and Water through Nafion Membranes. *J. Power Sources* **2004**, *130*, 22-29.

S8.   Martínez, L.; Andrade, R.; Birgin, E. G.; Martínez, J. M. PACKMOL: A Package for Building Initial Configurations for Molecular Dynamics Simulations. *J. Comput. Chem.* **2009**, *30*, 2157-2164.

S9.   Jewett, A. I.; Zhuang, Z.; Shea, J.-E. Moltemplate a Coarse-Grained Model Assembly Tool. *Biophys. J.* **2013**, *104*, 169a

S10.   Plimpton, S. Fast Parallel Algorithms for Short – Range Molecular Dynamics. *J. Comput. Phys.* **1995**, *117*, 1-19.

S11.   Jorgensen, W. L.; Chandrasekhar, J.; Madura, J. D.; Impey, R. W.; Klein, M. L. Comparison of Simple Potential Functions for Simulating Liquid Water. *J. Chem. Phys.* **1983**, *79*, 926-935.

S12. Ryckaert, J. P.; Ciccotti, G.; Berendsen, H. J. C. Numerical integration of the Cartesian Equations of Motion of a System with Constraints: Molecular Dynamics of n-Alkanes. *J. Comput. Phys.* **1977**, *23*, 327-341.

S13. Wang, J.; Wolf, R. M.; Caldwell, J. W.; Kollman, P. A.; Case, D. A. Development and Testing of a General Amber Force Field. *J. Comput. Chem.* **2004**, *25*, 1157-1174.

S14. Humphrey, W.; Dalke, A.; Schulten, K. VMD: Visual Molecular Dynamics. *J. Mol. Graph.* **1996**, *14*, 33-38.

S15. Gaussian 09, Revision A.02, M. J. Frisch, G. W. Trucks, H. B. Schlegel, G. E. Scuseria, M. A. Robb, J. R. Cheeseman, G. Scalmani, V. Barone, G. A. Petersson, H. Nakatsuji, X. Li, M. Caricato, A. Marenich, J. Bloino, B. G. Janesko, R. Gomperts, B. Mennucci, H. P. Hratchian, J. V. Ortiz, A. F. Izmaylov, *et al.*, Gaussian, Inc., Wallingford CT, 2016.

S16. Weigend, F.; Ahlrichs, R. Balanced Basis Sets of Split Valence, Triple Zeta Valence and Quadruple zeta Valence Quality for H to Rn: Design and Assessment of Accuracy. *Phys. Chem. Chem. Phys*. **2005**, *7*, 3297–305.

S17. Marenich, A. V.; Cramer, C. J.; Truhlar, D. G. Universal Solvation Model Based on Solute Electron Density and on a Continuum Model of the Solvent Defined by the Bulk Dielectric Constant and Atomic Surface Tensions. *J. Phys. Chem. B* **2009**, *113*, 6378-6396.

S18. Cances, M. T.; Mennucci, V.; Tomasi, J. A New Integral Equation Formalism for the Polarizable Continuum Model: Theoretical Background and Applications to Isotropic and Anisotropic Dielectrics. *J. Chem. Phys.* **1997**, *107*, 3032-3041.

S19. Tomasi, J.; Mennucci, B.; Cammi, R. Quantum Mechanical Continuum Solvation Models. *Chem. Rev.* **2005**, *105*, 2999-3093.